The role of hydrogen in the optimal design of off-grid hybrid renewable energy systems

Journal of Energy Storage 46 (2022) 103893

Contents lists available at ScienceDirect

Journal of Energy Storage

journal homepage: www.elsevier.com/locate/est

Research Papers

The role of hydrogen in the optimal design of off-grid hybrid renewable energy systems

Paolo Marocco *, Domenico Ferrero, Andrea Lanzini, Massimo Santarelli

Department of Energy, Politecnico di Torino, Corso Duca degli Abruzzi 24, 10129 Torino, Italy

ARTICLE INFO

Keywords:
Electrolysis
Hydrogen
Battery
Energy storage
CO_2 emissions
Off-grid

ABSTRACT

The optimal design of off-grid hybrid renewable energy systems (HRESs) is a challenging task, which often involves conflicting goals to be faced. In this work, levelized cost of energy (LCOE) and CO_2 emissions have been addressed simultaneously by using the ε-constraint method together with the particle swarm optimization (PSO) algorithm. Cost-emissions Pareto fronts of different HRES configurations were developed to gain greater awareness about the potential of renewable-based energy systems in off-grid applications. Various combinations of the following components were investigated: photovoltaic panels, wind turbines, batteries, hydrogen and diesel generators. The hydrogen-based system comprises an electrolyzer to convert the excess renewable energy into hydrogen, a pressurized tank for H_2 storage and a fuel cell for the reconversion of hydrogen into electricity during renewable energy deficits. Electrolyzer and fuel cell devices were modelled by means of part-load performance curves. Size-dependent costs and component lifetimes as a function of the cumulative operational duty were also considered for a more accurate techno-economic assessment. The proposed methodology was applied to the Froan islands (Norway), which were chosen as a reference case study since they are well representative of many other insular microgrid environments in Northern Europe. Results from the sizing simulations revealed that energy storage devices are key components to reduce the dependency on fossil fuels. In particular, the hydrogen storage system is crucial in off-grid areas to enhance the RES penetration and avoid a sharp increase in the cost of energy. Hydrogen, in fact, allows the battery and RES technologies not to be oversized, thanks to its cost-effective long-term storage capability. Concerning the extreme case with no diesel, the cheapest configuration, which includes both batteries and hydrogen, has an LCOE of 0.41 €/kWh. This value is around 35% lower than the LCOE of a system with only batteries as energy storage.

1. Introduction

Off-grid electrification in remote areas by means of renewable-based energy systems is needed to achieve main sustainable energy goals [1]. The rapid decline in technology costs is making renewable energy solutions a cost-competitive choice to extend electricity access in many unelectrified areas [2]. There is great potential to hybridize or even replace off-grid diesel-based systems with renewable energy generators [3]. Relying on local renewable energy sources (RESs) can represent an eco-friendly and cost-effective solution to release the off-grid community from the dependence on fossil fuels or to avoid unreliable and excessively expensive grid connections [4]. However, because of the fluctuating behavior of variable RESs (such as solar and wind), electrical energy storage (EES) systems should be considered to achieve high RES penetration levels [5,6]. Batteries are generally the first choice as storage medium due to their high performance, flexibility and declining costs [7]. Hydrogen-based storage solutions can also become necessary to depend entirely on non-dispatchable RESs, thanks to their long-term storage capability [8,9].

Concerning off-grid areas, relying only on diesel generators can result in a high cost of energy [4,10]. Diesel-based power production is often not affordable because of the high operating costs due to geographical remoteness (with related transport issues) and highly fluctuating fuel prices [11,12]. On the other hand, energy systems that are based only on local RESs can also incur high costs due to the system oversizing, which is necessary to provide a reliable power supply service over the entire year [10,13]. The hybridization of the energy system can be an effective solution to reduce the levelized cost of energy (LCOE). Malheiro et al. [10] reported that the use of diesel generators (DGs) allowed the battery not to be oversized. In fact, the authors observed

* Corresponding author.
E-mail address: paolo.marocco@polito.it (P. Marocco).

https://doi.org/10.1016/j.est.2021.103893
Received 5 August 2021; Received in revised form 26 November 2021; Accepted 20 December 2021
Available online 4 January 2022

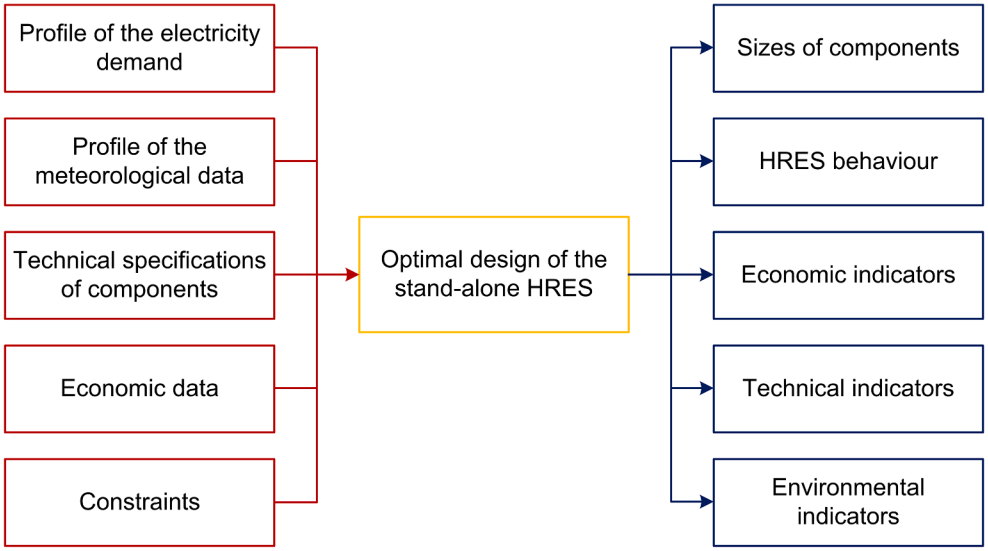

Fig. 1. Optimization framework developed in this work to perform the optimal design of stand-alone hybrid renewable energy systems.

that, without a diesel back-up system, the battery capacity became around three times higher than that required in the configuration with both batteries and DGs, with consequent significant increase in the LCOE value. Similar considerations were reported by Odou et al. [13], who investigated the techno-economic feasibility of hybrid renewable energy systems (HRESs) for sustainable rural electrification. They observed that the photovoltaics-diesel-battery configuration was the most cost-effective choice: batteries were in fact necessary to decrease the DG operational costs because of the reduced fuel consumption; at the same time, diesel genset allowed the battery capacity to be reduced by around 70% compared to the case with no diesel. Cai et al. [11] also showed that a system based on PV, batteries and diesel generators was cheaper than a system with only DGs. This is because the exploitation of solar energy reduced the consumption of the diesel fuel, which accounted for a considerable share of the LCOE. The inclusion of hydrogen in off-grid HRESs was also reported to be beneficial in decreasing the LCOE [14]. Dawood et al. [15] investigated different HRESs for remote communities and showed that a hybrid storage solution with both batteries and hydrogen was the most cost-effective option. Hydrogen, in fact, avoids the need for batteries with too large capacity [16]. Marchenko et al. [17] found that the storage hybridization resulted in the cheapest HRES configuration thanks to both the high efficiency of batteries and the long-term storage capacity of hydrogen-based systems. The economic benefits of combining batteries and hydrogen were also reported by Kalantari et al. [18], who investigated RES-based energy systems for application in remote mines.

The optimal design of hybrid renewable energy systems can be achieved by means of single-objective or multi-objective approaches. Multi-objective optimization problems (MOPs) should be considered when multiple and conflicting goals need to be addressed [19]. The objective functions of the optimization problem usually include system costs (e.g., in terms of LCOE) and environmental concerns such as operational CO_2 emissions [20,21], fossil fuel consumption [22] or equivalent life cycle CO_2 emissions [23,24]. According to the search approach, MOPs can be classified into: 1) Pareto-based techniques that employ ranking and selection in the population to generate the Pareto front and 2) non-Pareto-based techniques that involve the combination of objective functions and problem transformation [25]. Meta-heuristic methods such as genetic algorithms (GAs), evolutionary algorithms (EAs) and particle swarm optimization (PSO) algorithms are broadly used to solve HRES optimization problems [26]. Compared to the other meta-heuristic techniques, PSO may be easier to implement since it requires fewer parameters [27]. It is also characterized by great robustness and high convergence speed, which makes it a suitable choice for the design of energy systems [28].

The present work has been carried out under the EU project REMOTE [29], whose main goal is to demonstrate the economic and environmental advantages derived from adopting H_2-based storage solutions in off-grid areas. Cost of energy, environmental issues and reliability of the power supply have been addressed by means of the ε-constraint method, employing the PSO technique as optimization algorithm. Different HRES configurations were analysed by combining the following components: PV panels, wind turbines, diesel generators, hydrogen and batteries. Cost-emissions Pareto fronts of the various energy systems were derived and compared for an in-depth investigation of the role of hydrogen storage in scenarios characterized by different levels of energy independence. A sensitivity analysis on the diesel price was also carried out, being this value highly variable and impacting on the LCOE. The aim of this work is to provide a wide overview about stand-alone energy systems in remote environments, investigating the role of hydrogen in the HRES optimal design. The sizing methodology was applied to the Froan archipelago, which is located off the west coast of Norway and currently interconnected to mainland by an outdated sea cable that needs to be replaced. The replicability potential is very high considering plenty of minor islands in Northern Europe in the same situation.

The structure of this work is as follows: Section 2 reports the modeling of the hybrid energy system together with its control strategy. The design optimization approach is then defined in Section 3. Section 4 introduces the reference case study that has been selected for the techno-economic analysis. Section 5 shows the main sizing results and related discussion. Finally, major conclusions are summed up in Section 6.

2. HRES modeling and operation

The general layout of the proposed optimization framework is shown in Fig. 1, where the main input and output data are reported. Input parameters include: time series of electrical demand and meteorological data (ambient temperature, solar irradiance, wind velocity), technical specifications of the HRES components (efficiency curves, modulation ranges, etc.), economic data (investment, operation, maintenance and replacement costs, fuel price, discount rate) and constraints (reliability of the energy system, periodicity in the storage levels, CO_2 emissions, maximum size of the components). The main outputs of the optimization problem are as follows: the optimal sizes of all the HRES components, the behavior of the energy system over the selected time horizon (renewable energy usage, load coverage, power profiles), economic

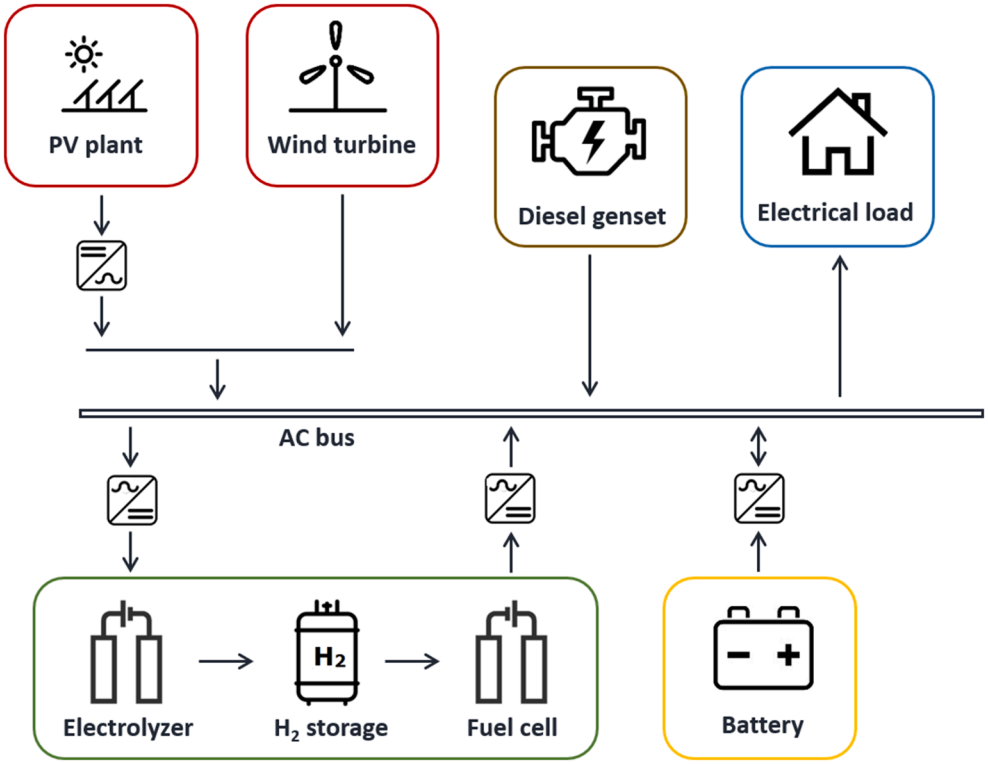

Fig. 2. General layout of the hybrid renewable energy system.

indicators (levelized cost of energy, net present cost), technical indicators (lifetime of components, etc.) and environmental indicators (amount of CO_2 that has been released during the HRES operation).

In the following sub-sections, the system configuration and the mathematical models of each component of the off-grid system will be discussed.

2.1. HRES architecture

The general layout of the hybrid renewable energy system is shown in Fig. 2. It comprises the following components: photovoltaic panels (PV), wind turbines (WT), batteries (BT), a hydrogen-based power-to-power (P2P) system and a diesel generator (DG), which are connected to an AC busbar [30], as in the Norwegian demo site of the REMOTE project [29].

The H2-based P2P system includes an electrolyzer (EL) for the conversion of electricity into hydrogen, a pressurized hydrogen tank (HT) to store the produced hydrogen gas and a fuel cell (FC) for the reconversion of H_2 into electricity. Different HRES configurations (obtained from the general layout by including different subsets of the above-listed components) were analysed in this work to better investigate the importance of EES hybridization under different fossil fuel-based cases.

2.2. PV system

The solar PV generation was computed as follows [22]:

$$P_{PV}(t) = f_{PV} \cdot P_{PV,rated} \cdot \frac{G(t)}{G_{STC}} \cdot \left[1 + \alpha_P \cdot \left(T_{cell}(t) - T_{cell,STC}\right)\right] \quad (1)$$

where P_{PV} (in kW) is the power delivered by PV panels, $P_{PV,\ rated}$ (in kW) is the rated power of the PV system, G (in kW/m^2) is the incident radiation over the PV panel tilted surface, G_{STC} (1 kW/m^2) is the incident radiation at standard test conditions (STC), T_{cell} (in °C) is the PV cell temperature, $T_{cell,STC}$ (25 °C) is the PV cell temperature under STC, α_P (in 1/K) is the temperature coefficient of power and finally f_{PV} is the derating factor accounting for reduced PV output in real-world operating conditions.

The following relationship was used to evaluate the PV cell temperature [31]:

$$T_{cell}(t) = T_a(t) + \frac{G(t)}{0.8} \cdot \left(T_{cell,NOCT} - 20\right) \quad (2)$$

where T_a (in °C) is the ambient temperature and $T_{cell,NOCT}$ (in °C) is the nominal operating cell temperature. The procedure applied to derive the incident radiation G is described in detail in the Appendix A. Main meteorological data were taken from PVGIS tool referring to a typical meteorological year (TMY) [32].

2.3. Wind turbine generators

The output power of the wind turbine was computed by employing a characteristic power versus wind speed curve, as the one described below [33]:

$$P_{WT}(t) = \begin{cases} 0, & \text{if } v_w(t) \le v_{w,ci} \\ P_{WT,rated} \cdot \dfrac{v_w^3(t) - v_{w,ci}^3}{v_{w,r}^3 - v_{w,ci}^3}, & \text{if } v_{w,ci} \le v_w(t) \le v_{w,r} \\ P_{WT,rated}, & \text{if } v_{w,r} \le v_w(t) \le v_{w,co} \\ 0, & \text{if } v_w(t) \ge v_{w,co} \end{cases} \quad (3)$$

where $v_{w,ci}$, $v_{w,co}$, and $v_{w,r}$ (in m/s) correspond to the cut-in, cut-out and rated wind speed, respectively. $P_{WT}(t)$ (in kW) is the produced wind power, whereas $P_{WT,rated}$ (in kW) is the rated power of the machine.

TMY wind speed data (with hourly resolution) were taken from [32], referring to a reference height (h_{ref}) of 10 m. They need thus to be corrected to the turbine height (h_{WT}):

$$v_w(t) = v_{w,ref}(t) \cdot \left(\frac{h_{WT}}{h_{ref}}\right)^{\alpha} \quad (4)$$

where $v_{w,ref}$ (in m/s) is the wind speed measured at the reference height and α is the exponent law coefficient. The latter depends on the surface topology. A value of 0.14 was adopted, which is typical for flat surfaces [52].

2.4. Battery storage system

The battery component was treated as an energy tank, modifying its charge level based on the power exchanged with the bus bar. The state-of-charge (SOC) parameter, which represents the ratio of the stored energy to the battery rated capacity, was used to describe the state of the battery as follows:

$$SOC(t) = SOC(t-1)\cdot(1-\sigma_{BT}) + \frac{P_{BT,ch}(t-1)\cdot\Delta t\cdot\eta_{BT,ch}\cdot\eta_{rect}}{Cap_{BT}} - \frac{P_{BT,dc}(t-1)\cdot\Delta t}{\eta_{inv}\cdot\eta_{BT,dc}\cdot Cap_{BT}} \quad (5)$$

where σ_{BT} is the hourly self-discharge rate of the battery, $P_{BT,ch/dc}$ (in kW) is the battery charging/discharging power, $\eta_{BT,ch/dc}$ is the battery charging/discharging efficiency, η_{inv} is the inverter efficiency, η_{rect} is the rectifier efficiency and Cap_{BT} (in kWh) is the capacity of the battery.

The SOC of the battery should also be bounded between a minimum and maximum value:

$$SOC_{min} \le SOC(t) \le SOC_{max} \quad (6)$$

The lower SOC threshold was imposed to avoid damaging the storage bank by excessive discharge.

In the present work, the lithium-ion technology was considered for the battery component, given its better performance compared to the lead-acid alternative [14].

2.5. Hydrogen-based P2P system

The hydrogen-based P2P system comprises an electrolyzer operating up to 30 bar, a pressurized hydrogen storage tank (maximum storage pressure of 28 bar) and a fuel cell working at ambient pressure. No compression step is therefore required between the electrolyzer and the storage. The proton-exchange membrane (PEM) technology was assumed for both the EL and FC components. The PEM option is in fact recommended when dealing with variable renewable energy sources (as in the case of wind generation) because of its good dynamic behavior [34].

The level-of-hydrogen (LOH) in the tank, which is defined as the ratio of the stored H_2 energy to the H_2 tank capacity, was obtained as:

$$LOH(t) = LOH(t-1) + \frac{P_{EL}(t-1)\cdot\Delta t\cdot\eta_{EL}}{Cap_{H2}} - \frac{P_{FC}(t-1)\cdot\Delta t}{\eta_{FC}\cdot Cap_{H2}} \quad (7)$$

where $P_{EL/FC}$ (in kW) is the electrolyzer/fuel cell operating power, $\eta_{EL/FC}$ is the efficiency of the electrolyzer/fuel cell system (including also BOP losses) and Cap_{H2} (in kWh) is the rated capacity of the hydrogen tank (in terms of energy content of hydrogen).

At any time-interval, the following constraints on the lower and upper limit of the LOH should be respected:

$$LOH_{min} \le LOH(t) \le LOH_{max} \quad (8)$$

The minimum LOH value was chosen to effectively overcome downstream pressure drops and allow the fuel cell to be fed with hydrogen. The LOH_{min} can be derived as the ratio between the minimum and maximum HT pressure.

Electrochemical devices were imposed to work within specific boundaries for a safe and efficient operation. A minimum operating power of 10% and 6% (defined as percentage of the rated power) was set for the electrolyzer and fuel cell, respectively [4]. Too low partial loads may in fact lead to safety issues because of the risk of explosive gas mixtures (related to hydrogen cross-diffusion) [35]. Reduced current densities are also responsible for an enhancement of the chemical degradation of the PEM membrane [36]. Moreover, the low-load operation also causes the efficiency to drop sharply because of the prevalence of the BOP consumption [14].

Variability in RES production and load requires that the fuel cell and the electrolyzer continuously adapt their operating point to reliably cover the load demand and store the surplus renewable energy. Part-load performance curves are thus recommended to get a more accurate techno-economic assessment. In this work, efficiency curves, taken from Ref. [14], were used to model the performance of the hydrogen-based devices. They were implemented within the optimization process by means of polynomial functions.

2.6. Diesel generator

The diesel fuel consumption was computed according to the following relationship [37–39]:

$$cons_{DG}(t) = a_{DG}\cdot P_{DG,rated} + b_{DG}\cdot P_{DG}(t) + cons_{start,DG} \quad (9)$$

where $cons_{DG}$ (in L/h) is the fuel consumption, $P_{DG,rated}$ (in kW) is the DG rated power, P_{DG} (in kW) is the DG operating power and $cons_{start,DG}$ (in L/start-up) represents the DG start-up penalty. The terms a_{DG} (in L/kWh) and b_{DG} (in L/kWh) correspond to the coefficients of the fuel consumption curve. They were set equal to 0.08415 L/kWh and 0.246 L/kWh, respectively.

The term $cons_{start,DG}$ was expressed as follows:

$$cons_{start,DG} = F_{start}\cdot\left(a_{DG}\cdot P_{DG,rated} + b_{DG}\cdot P_{DG,rated}\right) \quad (10)$$

where F_{start} represents a factor accounting for the extra fuel due to the DG start-up. Its value is usually lower than 0.083, equal to around 5 min at rated power [38,39]. In the present work, we considered a value of 0.067, representing approximately 4 min of continuous high-load operation [40].

A minimum service level was imposed to the diesel generator to avoid its operation with low efficiency:

$$P_{DG}(t) \ge y_{DG,min}\cdot P_{DG,rated} \quad (11)$$

where $y_{DG,min}$ is the minimum output power, set to 30% of the rated power [10,38].

2.7. Energy management of the HRES

An energy management strategy (EMS) was developed to perform simulations of the hybrid renewable energy system over a 1 yearlong time horizon with hourly resolution. In a configuration with storage hybridization (i.e., both battery and hydrogen), batteries act as shorter-term storage whereas hydrogen works as longer-term storage, intervening when the maximum or minimum BT SOC values are reached. The battery component is thus used to mitigate RES intermittency and to protect the H_2-based components from too frequent start-ups and shut-downs, which would negatively affect their lifetime.

The detailed logical block diagram of the adopted EMS can be found in [4]. However, we modified it in the present study to include the operation of the diesel genset.

Whenever the load demand is greater than the renewable power, priority of intervention is the following: battery discharging first, then fuel cell operation and finally diesel generator operation. The same priority rule is kept also when one of these components (i.e., BT, FC and DG) is not included within the HRES. The diesel generator (if present) is thus operated as a final back-up device and according to a load following dispatch strategy, i.e., it is operated (compatibly with its modulation range) so as to cover the unmet fraction of primary load. In case the load to be covered by the DG is lower than the DG minimum power, the diesel generator operates at its minimum power to feed the load (the FC/BT

Table 1
Technical input parameters for the HRES components.

Component	Value	Ref.
PV power plant		
Derating factor, f_{PV}	0.86	
Nominal operating cell temperature, $T_{cell,NOCT}$	44 °C	[57]
Temperature coefficient, α_P	−0.003 1/K	[57]
PV surface slope, β	49°	[32]
PV surface azimuth, ϕ	2°	[32]
Albedo of the ground, ρ_g	0.2	[58]
Incident irradiance at STC, G_{STC}	1 kW/m^2	
PV cell temperature at STC, $T_{cell,STC}$	25 °C	
Lifetime	20 yr	
Wind power plant		
Turbine height, h_{WT}	30 m	[59]
Wind speed reference height, h_{ref}	10 m	[32]
Exponent law coefficient, α	0.14	[42]
Cut-in wind speed, $v_{w,ci}$	3 m/s	[59]
Cut-out wind speed, $v_{w,co}$	25 m/s	[59]
Rated wind speed, $v_{w,r}$	13 m/s	[59]
Lifetime	20 yr	
Diesel generator		
Fuel consumption curve parameter, a_{DG}	0.08415 L/kWh	[37–39]
Fuel consumption curve parameter, b_{DG}	0.246 L/kWh	[37–39]
Start-up extra fuel parameter, F_{start}	0.067	[40]
Minimum power, $y_{DG,min}$ (% of rated power)	30%	[10,38]
CO_2 emissions, $c_{CO_2,DG}$	3 kg/L	[44]
Operating hours (over lifetime), $N_{h,tot,DG}$	20,000 h	[44]
BOP lifetime	20 yr	
Li-ion battery		
Charging efficiency, $\eta_{BT,ch}$	0.95	[60,61]
Discharging efficiency, $\eta_{BT,dc}$	0.95	[60,61]
Self-discharge, σ_{BT}	5%/month	[41]
Minimum SOC, SOC_{min}	0.2	[41,61]
Maximum SOC, SOC_{max}	1	
Battery bank lifetime	From the lifetime curve	[62]
BOP lifetime	20 yr	
Hydrogen tank		
Minimum pressure, p_{min}	3 bar	[4]
Maximum pressure, p_{max}	28 bar	[4]
Minimum LOH, LOH_{min}	p_{min}/p_{max}	
Maximum LOH, LOH_{max}	1	
Lifetime	20 yr	
PEM electrolyzer		
Minimum power (% of rated power)	10%	[63]
Efficiency, η_{EL}	Efficiency curve	[14]
Operating hours (over lifetime), $N_{h,tot,EL}$	40,000 h	[49]
On-off cycle number (over lifetime), $N_{st,tot,EL}$	5,000	[64]
BOP lifetime	20 yr	
PEM fuel cell		
Minimum power (% of rated power)	6%	[4]
Efficiency, η_{FC}	Efficiency curve	[14]
Operating hours (over lifetime), $N_{h,tot,FC}$	30,000 h	[42,65]
On-off cycle number (over lifetime), $N_{st,tot,FC}$	10,000	[66]
BOP lifetime	20 yr	

power is lowered accordingly and the excess power, if any, is used to charge the battery).

When the load demand is lower than the available renewable power, the energy surplus from RES is first stored in batteries (if present), then converted into H_2 by means of electrolyzers (if present) and finally curtailed.

3. HRES optimal sizing

3.1. Sizing approach

The optimal sizing was performed by using the PSO technique. The main goal is to identify the system configuration (i.e., sizes of PV, WT, BT, EL, FC, HT and DG components), that allows the LCOE to be minimized.

The general structure of the optimization problem is summarized below:

$$\begin{cases} min(LCOE) \\ C1: \ UL \le UL_{target} \\ C2: \ SOC(t_{end}) \ge SOC(t_{in}) \\ C3: LOH(t_{end}) \ge LOH(t_{in}) \\ C4: \ m_{CO_2,op} \le m_{CO_2,op,target} \end{cases} \quad (12)$$

C1-C4 are the constraints that have been imposed in the optimization process. C1, which corresponds to the reliability constraint, ensures that the unmet load (UL) index is not higher than a certain target value. The UL is defined as the ratio of the total not served energy to the total energy demand over the selected time horizon T (i.e., 1 year):

$$UL(\%) = \frac{\sum_{t=1}^{T} P_{NS}(t) \cdot \Delta t}{\sum_{t=1}^{T} P_{LD}(t) \cdot \Delta t} \quad (13)$$

where P_{NS} (in kW) is the not served power and P_{LD} (in kW) is the load demand. A value of 0% was set for UL_{target} so that the electrical demand is covered at all times by the stand-alone power system [22,41].

The storage autonomy constraints C2 and C3 ensure that the energy in the storage systems at the end of the year is greater than or equal to that present at the beginning of the simulation (in this work, a value of 0.5 was chosen for the initial SOC and LOH) [42,43]. Finally, C4 refers to the constraint on the yearly amount of CO_2 that is released by the operation of the HRES. This value is due to the fuel that is consumed by the diesel generator [20,21]. The annual CO_2 emitted during HRES operation was computed as follows:

$$m_{CO_2,op} = \sum_{t=1}^{T} cons_{DG}(t) \cdot c_{CO_2,DG} \quad (14)$$

where $cons_{DG}$ (in L/h) is the diesel fuel consumption (evaluated according to Eq. (9)) and $c_{CO_2,DG}$ (in kg/L) is the related CO_2 emission coefficient, which lies in range 2.4–3.5 kg/L [44]. The $m_{CO_2,op}$ quantity is therefore strictly correlated to the energy independence of the site (i.e., amount of fuel that should be periodically transported to the island to run the diesel genset).

Cost-emissions Pareto fronts were derived for different system configurations. The ε-constraint method was employed to minimize both the LCOE and CO_2 emissions of the system [27,45]. According to this technique, the multi-objective optimization problem is solved by optimizing one objective and treating the remaining ones as constraints. First, two different single-objective optimization problems were performed to find the upper ($m_{CO_2,op,max}$) and lower ($m_{CO_2,op,min}$) limits of the annual CO_2 emissions. In more detail, in order to evaluate the $m_{CO_2,op,max}$ value, a single-objective minimum-cost optimization was carried out, independently of the CO_2 emissions, as follows:

$$\begin{cases} min(LCOE) \\ C1: \ UL \le UL_{target} \\ C2: \ SOC(t_{end}) \ge SOC(t_{in}) \\ C3: LOH(t_{end}) \ge LOH(t_{in}) \end{cases} \quad (15)$$

The $m_{CO_2,op,min}$ value was instead quantified by performing a single-objective minimum-emissions optimization, independently of the costs, as reported below:

Table 2
Economic input parameters for the HRES components.

Component	Value	Ref.
PV power plant		
Investment cost	1,547 €/kW	[4]
Fixed OM costs (% of Inv. cost)	24 €/kW/yr	[4]
Wind power plant		
Investment cost	1,175 €/kW	[67]
Fixed OM costs (% of Inv. cost)	3%/yr	[4]
Diesel generator		
Investment cost	420 €/kW	[41]
Replacement cost	420 €/kW	[41]
Variable OM costs, $c_{OM,\ DG,op}$	0.4 €/h	[41]
Fuel cost, $cost_{fuel}$	2 €/L (ref. case)	[4]
Li-ion battery		
Investment cost (system)	550 €/kWh	[4,41]
Replacement cost (battery module)	275 €/kWh	[68]
Fixed OM costs	10 €/kWh/yr	[61]
Hydrogen tank		
Investment cost	470 €/kg	[49]
Fixed OM costs (% of Inv. cost)	2%/yr	[49]
PEM electrolyzer		
Ref. specific investment cost, $c_{inv,ref}$	4,600 €/kW	[47]
Ref. rated size, $P_{rated,ref}$	50 kW	[47]
Cost exponent, n_{inv}	0.65	[47]
Replacement cost (% of Inv. Cost)	26.7%	[69]
Fixed OM costs (% of Inv. Cost)	1/3•4%/yr	[49]
Variable OM costs (% of Inv. Cost)	2/3•4%/yr	[49]
PEM fuel cell		
Ref. specific investment cost, $c_{inv,ref}$	3,947 €/kW	[48]
Ref. rated size, $P_{rated,ref}$	10 kW	[48]
Cost exponent, n_{inv}	0.7	[14]
Replacement cost (% of Inv. Cost)	26.7%	[69]
Fixed OM costs (% of Inv. Cost)	1/3•4%/yr	[49]
Variable OM costs (% of Inv. Cost)	2/3•4%/yr	[49]
Other assumptions		
Real discount rate, d	4.9%	[4]
Project lifetime, n	20 yr	[55]

$$\begin{cases} min\left(m_{CO_2,op}\right) \\ C1:\ UL \le UL_{target} \\ C2:\ SOC(t_{end}) \ge SOC(t_{in}) \\ C3: LOH(t_{end}) \ge LOH(t_{in}) \end{cases} \quad (16)$$

The CO_2 emission interval thus obtained was divided into n steps. The Pareto front was then built by resolving n single-objective optimization problems that minimize the LCOE, while subject to a constraint on the annual CO_2 emission (which is varied between $m_{CO_2,op,min}$ and $m_{CO_2,op,max}$). The structure of each single-objective optimization is outlined in Eq. (12).

Concerning the PSO algorithm, the population size was set to 100. A value of 2 was chosen for both the cognitive and social parameters [46].

The size of each HRES component was allowed to vary between zero and a certain upper boundary (UB), which was chosen so as not to be a constraint on the optimal size. According to the scenario under analysis, the UB of some components was set to zero (e.g., UB of the battery size in the H_2 scenario and UB of the hydrogen-based equipment in the BT scenario).

3.2. LCOE estimation

Techno-economic data, that are required as input for the modeling of the HRES and for the evaluation of the LCOE, are listed in Table 1 and Table 2 (main specifications of PV, battery and hydrogen-based components were taken from Ref. [14]) .

The following relationship was used for the estimation of the LCOE (in €/kWh):

$$LCOE = \frac{C_{NPC,tot}}{\sum_{j=1}^{n} \frac{E_{tot,j}}{(1+d)^j}} \quad (17)$$

where $C_{NPC,tot}$ (in €) is the overall system net present cost (NPC), $E_{tot,j}$ (in kWh) is the load demand covered by the HRES during j-th year, n is the lifetime of the project (set to 20 years in this study) and d is the real interest rate (which is a function of the nominal interest rate and the annual inflation rate).

The system NPC was derived as follows (with i = PV, WT, EL, FC, BT, HT, DG and k = EL, FC, BT, DG):

$$C_{NPC,tot} = \sum_i C_{inv,i,0} + \sum_{j=1}^{n} \frac{\sum_k C_{rep,k,j} + \sum_i C_{OM,\ i,j}}{(1+d)^j} - \sum_k \frac{C_{sal,k,n}}{(1+d)^n} \quad (18)$$

where $C_{inv,i,0}$ (in €) is the investment cost of the i-th component at the beginning of the simulation, $C_{rep,k,j}$ (in €) is the replacement cost of the k-th component during the j-th year (it is null in case there is no replacement in that year), $C_{OM,\ i,j}$ (in €) is the operation & maintenance (OM) cost of the i-th component for the j-th year and finally, $C_{sal,k,n}$ (in €) is the salvage cost of the k-th component occurring at the end of the project lifetime.

Concerning investment costs, the following power function was employed for the electrolyzer and fuel cell [4]:

$$c_{inv} = \left(\frac{P_{rated}}{P_{rated,ref}}\right)^{n_{inv}} \cdot \frac{c_{inv,ref} \cdot P_{rated,ref}}{P_{rated}} \quad (19)$$

where c_{inv} (in €/kW) is the specific investment cost referred to an EL/FC system with rated power P_{rated} (in kW), $c_{inv,ref}$ (in €/kW) is the reference specific investment cost of a reference EL/FC system with rated power $P_{rated,ref}$ (in kW) and n_{inv} is the cost exponent of the power function. These parameters were derived by fitting the cost data reported in Refs. [47] and [48] and are suitable for kW-size H_2-based devices.

The investment cost of the compressed H_2 storage (of 470 €/kg) was taken from [49], which is in accordance with other studies from the literature [50–53]. Overall, the costs that have been chosen for the HRES components are also in line with the REMOTE partners' knowledge [4].

Replacement costs were assessed as a fraction of the investment cost. The values of the component lifetimes should be defined to estimate when replacements take place over the entire 20-year time horizon. In this study, lifetimes of components that may potentially be replaced (i.e., EL, FC, BT and DG) were computed based on how they operate over the reference year. In more detail, the lifespan of the EL/FC devices was determined from the yearly number of operating hours ($N_{h,yr,EL/FC}$) and start-ups ($N_{st,yr,EL/FC}$), according to the relationship reported in [14]. The battery duration was estimated by computing the lifetime throughput (from the battery lifetime curve) and dividing this value by the annual throughput (i.e., the yearly amount of energy flowing through the battery) [54]. The diesel genset life was finally evaluated from the ratio of the total amount of DG working hours ($N_{h,tot,DG}$) to the number of DG yearly working hours ($N_{h,yr,DG}$). The lifetime of the project was set as upper threshold for the lifetime of all the components of the HRES [14].

As shown in Eq. (18), a salvage cost term was also included for all the components that may be subject to replacement. The salvage value, which depends on the replacement cost, was computed supposing that it is directly proportional to the remaining lifetime of the component.

A fixed OM cost was considered for the PV, WT, BT and HT components. OM costs of the electrolyzer and fuel cell were instead assumed to consist of a fixed and variable contribution (the variable term was supposed to be proportional to the EL/FC operating time) [49]. The OM cost of the diesel generator was evaluated according to the amount of fuel that is consumed and to the number of DG operating hours:

$$C_{OM,\ DG} = \sum_{t=1}^{T} cons_{DG}(t) \cdot cost_{fuel} + c_{OM,\ DG,op} \cdot N_{h,yr,DG} \quad (20)$$

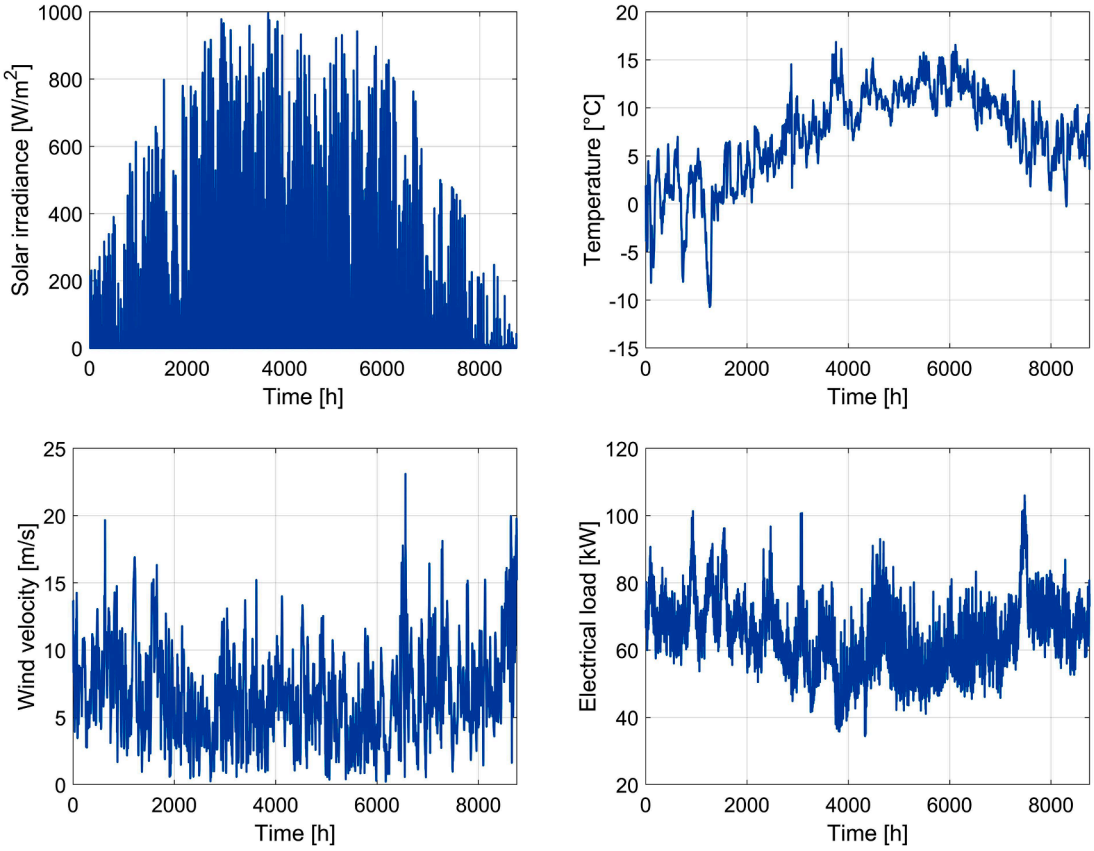

Fig. 3. Input meteorological and load data profiles over a reference year in Froan: solar irradiance (total irradiance over the PV panel tilted surface), ambient temperature, wind velocity (10 m height) and electrical load.

Table 3
Main sizing results and technical KPIs referred to the 100% RES-based HRES.

Sizing results						
$P_{WT,rated}$ [kW]	$P_{PV,rated}$ [kW]	Cap_{BT} [kWh]	$P_{EL,rated}$ [kW]	$P_{FC,rated}$ [kW]	Cap_{HT} [kg]	LCOE [€/kWh]
483	318	277	115	90	718	0.410
Technical KPIs						
$N_{h,yr,EL}$ [h]	$N_{st,yr,EL}$ [-]	L_{EL} [yr]	$N_{h,yr,FC}$ [h]	$N_{st,yr,FC}$ [-]	L_{FC} [yr]	L_{BT} [yr]
3294	293	7	2022	234	11	12

where $C_{OM,\ DG}$ (in €/yr) is the DG OM cost, $cost_{fuel}$ (in €/L) is the price of the diesel fuel, $c_{OM,\ DG,op}$ (in €/h) is the specific OM cost associated to DG operation and $N_{h,yr,DG}$ (in h) is the number of DG operating hours over the reference year.

The fuel price is generally high in off-grid remote locations [55]. A value of around 2 €/L is suggested in Refs. [4,41,56]. Alberizzi et al. [56] reported that the fuel price varies from approximately 1.4 €/L up to 3 €/L in remote areas. In the present work, a sensitivity analysis of the diesel price in the range from 1 to 3 €/L was performed to better investigate its influence on the HRES optimal sizing (2 €/L was considered for the reference case).

4. Froan case study

The Froan archipelago has been considered in the present analysis as case study to perform the techno-economic assessment. It consists of 4 islands close to the coast, near Trondheim (Norway), and connected to the mainland grid through an outdated sea cable, whose expected remaining lifespan is around 5 years [3]. The replacement of the sea cable would require expensive (and invasive) engineering and civil works. Alternative solutions need therefore to be considered to provide electrical power to the site. An immediate choice could be the installation of an on-site diesel generator; however, its usage should be limited as much as possible being the Froan archipelago a nature reserve and conservation area. Energy production based on local RESs thus represents an interesting and eco-friendly alternative. Electrical energy storage systems should be accounted for within the RES-based solution to enhance the independence of Froan from imported diesel fuel. EES devices would in fact improve the exploitation of local renewable energy and mitigate the variability in renewable energy production and load demand, thus securing the power supply throughout the entire year.

Main meteorological and load hourly profiles over a reference year for the Froan site are reported in Fig. 3 [32,70]. Load data were directly provided by the end-user of the selected site [70]. The annual electrical demand is approximately 561 MWh. The peak load is slightly higher than 100 kW and the average daily load demand accounts for about 1, 538 kWh. Electricity consumption in summer is primarily due to tourism, whereas during winter the power consumption is mainly due to heating and, to a lesser extent, to lightning.

5. Results and discussion

The optimal sizing was first carried out focusing on a system fully relying on local wind and solar sources (i.e., 100% RES-based system). Main sizing outcomes are reported in Table 3: it can be seen that the optimal fossil-fuel-free configuration is characterized by the hybridization of both power sources (PV and WT) and storage (BT and H_2). Even though solar energy is scarce in the selected site (which is typical for northern climates), it is economically convenient to install PV together with wind turbines. In fact, solar energy compensates for the reduced

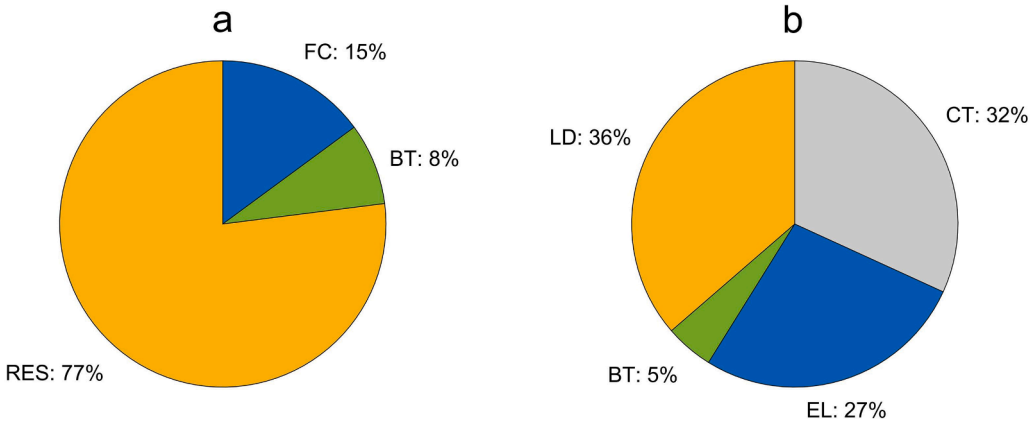

Fig. 4. Coverage of the yearly load (a) and usage of yearly RES production (b) for the 100% RES-based HRES.

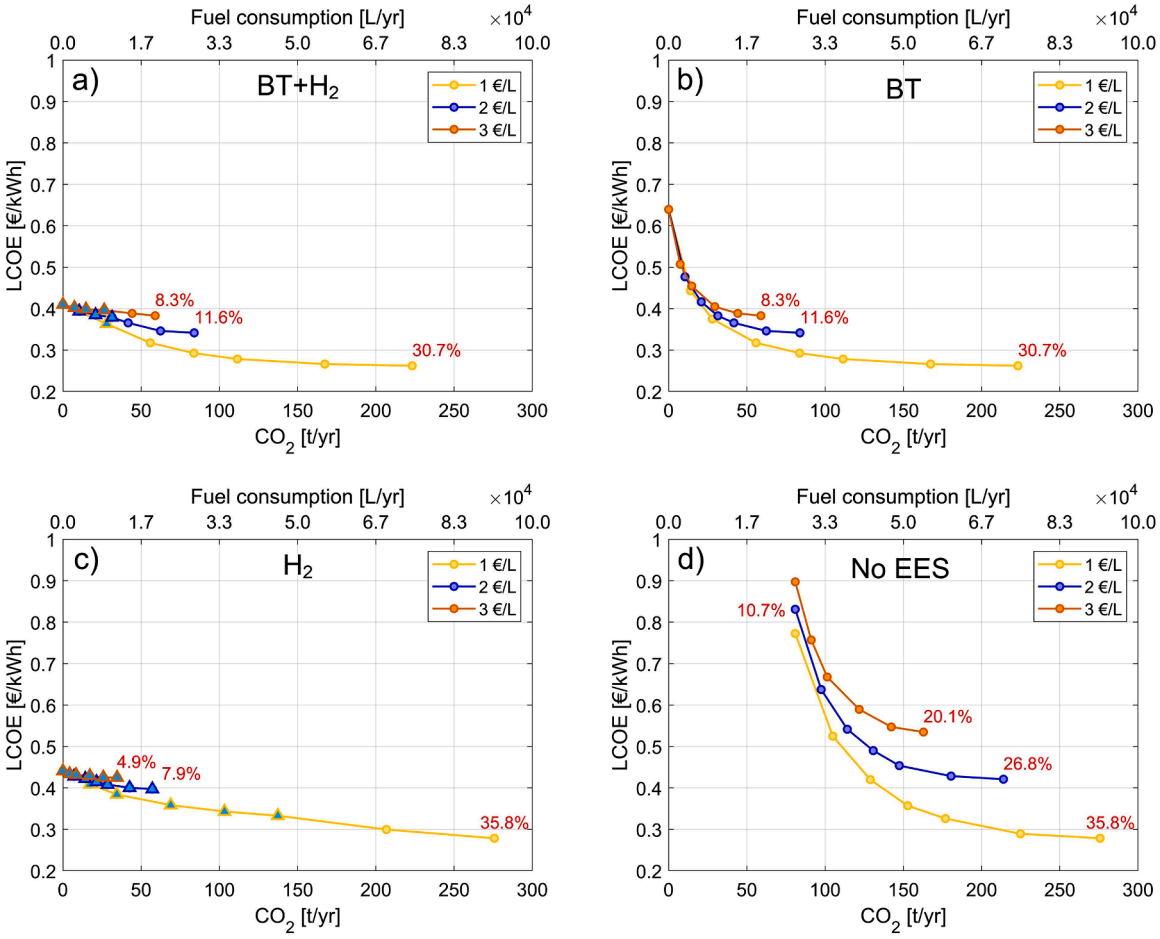

Fig. 5. Cost-emission Pareto fronts for a) BT + H_2, b) BT, c) H_2 and d) No EES scenarios. Light blue triangles correspond to configurations with the presence of hydrogen, whereas red coloured percentages represent DF values.

availability of the wind source during the summer period. It can also be noted that a large HT size is required to make the energy system 100% based on local RESs. The hydrogen-based storage system is crucial to deal with the seasonality of the RES supply and the electrical load. The level-of-hydrogen over the year is shown in Appendix B (Fig. B.1). The resulting system LCOE is about 0.410 €/kWh, which is lower than the cost of energy referred to an alternative scenario with sea cable replacement (approximately 0.630 €/kWh [4]). Technical key performance indicators (KPIs) are also shown in Table 3: according to the system simulation, battery modules and fuel cell stacks should be replaced once during the project, with lifetimes of 12 and 11 years, respectively; whereas the electrolyzer stack, whose lifetime is around 7 years, needs two replacements.

Main results from the energy balance simulations on a yearly basis are displayed in Fig. 4. As shown in Fig. 4a, most of the electrical load (approximately 77%) is covered by direct consumption of energy coming from the PV and WT. However, in order to make the site energy independent, the hybrid P2P system must intervene covering

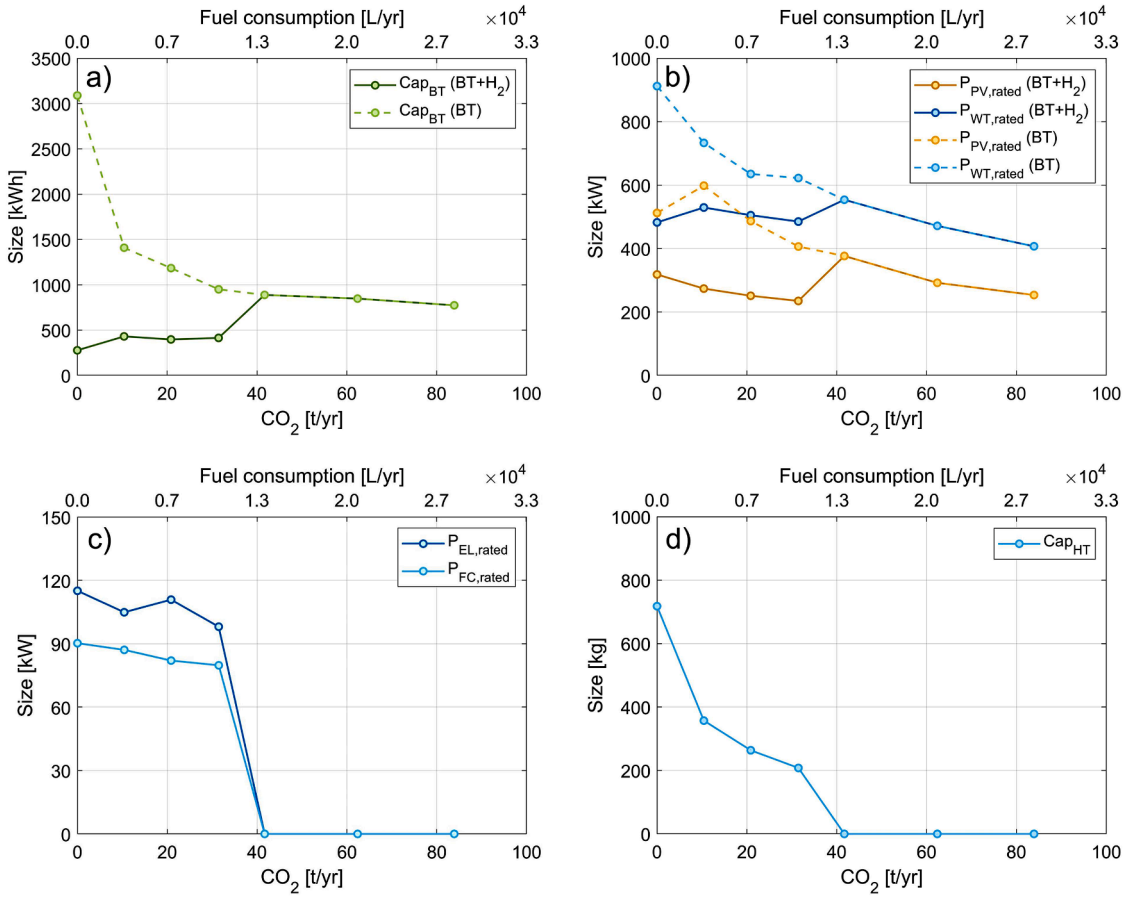

Fig. 6. a) Battery capacity in the BT+H_2 and BT scenarios; b) RES (PV and WT) rated power in the BT+H_2 and BT scenarios; c) EL and FC rated power in the BT+H_2 scenario; d) HT capacity in the BT+H_2 scenario. All figures are referred to the case with a diesel fuel cost of 2 €/L.

approximately 23% of the annual load, of which around two-thirds are met by the fuel cell and the remaining fraction by the battery component. Fig. 4b reports how the annual RES production is divided between load (direct consumption), battery storage, hydrogen storage through electrolysis and curtailment. The latter term accounts for around 32% of the overall renewable production. This value is high, but it is unavoidable in off-grid systems that aim to achieve the energy self-sufficiency by relaying completely on local RESs.

The sizing optimization was then performed including the diesel generator component to better investigate the role of hydrogen in the optimal design of stand-alone HRESs. Cost-emissions Pareto fronts were derived considering different system scenarios: 1) RES+DG+BT+H_2 (BT+H_2), 2) RES+DG+BT (BT), 3) RES+DG+H_2 (H_2) and finally 4) RES+DG (No EES). Main results of the four cases are reported in Fig. 5, where the LCOE is displayed as a function of the yearly CO_2 emissions (in tonnes per year) and fuel consumption (in litres per year). A sensitivity analysis on the diesel fuel cost in the range from 1 to 3 €/L was carried out for the sake of comparison. Diesel fraction (DF) values are also displayed for the cheapest configuration of each cost-emission curve. DF represents the fraction of the yearly electrical demand that is covered by the diesel generator (the remaining fraction is therefore covered by the renewable P2P system).

Fig. 5 shows that, for all the 4 scenarios, a reduction in the LCOE implies an increase in CO_2 emissions (or related fuel consumption). Concerning the hybrid storage scenario (Fig. 5a) and 2 €/L as fuel price, it was found that the most cost-effective configuration has an LCOE of around 0.34 €/kWh with approximately 84 tonnes of CO_2 released yearly by the system operation (the related DF value is around 11.6%). The LCOE of the cheapest configuration moves to 0.26 and 0.38 €/kWh when considering a fuel price of 1 and 3 €/L, respectively, which shows the high influence of this value on the cost of energy. By comparing Fig. 5a and b, it can be noted that the least expensive configurations are the same for the BT+H_2 and BT scenarios. This means that there is no need to include hydrogen when no constraints on the usage of diesel generators are imposed: the cost-optimal system is in fact composed of RESs (both PV and WT) together with batteries and diesel generators. By decreasing the amount of allowed CO_2 in the BT+H_2 scenario, it can be observed that the hydrogen storage system appears in the optimal system configuration at around 30–40 tonnes of CO_2 per year (light blue triangles in Fig. 5a). The cost of energy then slightly increases up to 0.41 €/kWh when a 100% RES-based system is achieved. Regarding instead a system that relies only on batteries as energy storage (Fig. 5b), by progressively limiting the operation of the diesel generator, the LCOE rises sharply to a maximum of 0.64 €/kWh. Hydrogen thus turns out to be necessary to limit the system costs when energy independence from fossil fuels is pursued. This is also confirmed by the LCOE trend of the H_2 scenario (Fig. 5c), which slowly increases by decreasing CO_2 emissions until reaching an LCOE of 0.44 €/kWh for the diesel-free configuration. Additional considerations about the effectiveness of H_2 in achieving cost-optimal HRES configurations can be found in Appendix B. Finally, Fig. 5d refers to a scenario with only RESs and diesel genset, without the inclusion of electrical energy storage devices. It is shown that the yearly CO_2 emissions cannot go below 81 tonnes per year, which corresponds to an DF of around 10.7%. The LCOE at this value of DF is in the 0.77–0.9 €/kWh range. For the sake of completeness, a system configuration with only DG was also simulated, resulting in an LCOE of 0.81 €/kWh (with a diesel price of 2 €/L) and approximately 648 tonnes of CO_2 per year. Energy storage systems are therefore essential to reduce the system costs

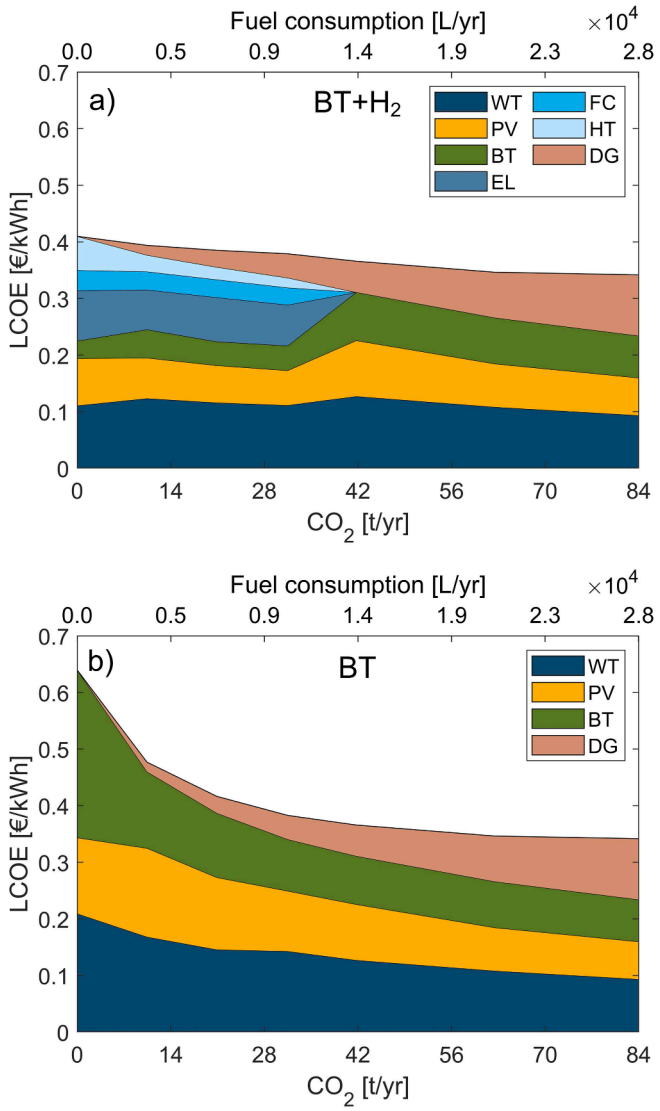

Fig. 7. LCOE breakdown for the BT+H_2 (a) and BT (b) scenarios as a function of the yearly CO_2 emissions and fuel consumption (referred to the case with a diesel fuel cost of 2 €/L).

and reach higher levels of RES penetration. It is also noteworthy that renewable configurations based EES devices are cost competitive compared to an alternative solution based on the sea cable replacement (whose LCOE is 0.630 €/kWh [4]).

Fig. 6 focuses on the BT+H_2 and BT scenarios to better understand the LCOE trends reported in Fig. 5. The cheapest configuration is characterized by the same system architecture for the two scenarios: around 254 kW of PV, 407 kW of WT, 774 kWh of BT and 90 kW of DG. By limiting the operation of the DG, the resulting LCOE increment is due to an increase in size of the EES and RES technologies. More specifically, concerning the BT scenario, the rated capacity of the battery increases abruptly, reaching a value of approximately 3,090 kWh for the configuration with no DG (which is approximately 4 times higher than the battery capacity with no CO_2 constraints). PV and WT sizes increase as well, moving from 254 to 512 kW (PV) and from 407 to 912 kW (WT). The system configuration of the BT+H_2 scenario is the same as that of the BT scenario until around 40 tonnes of CO_2 per year (i.e., 120,000 L of diesel fuel per year). Below this CO_2 value, installing an H_2-based storage system becomes economically convenient. The presence of hydrogen is in fact useful to avoid the oversizing of the battery component (Fig. 6a) thanks to the low-cost high-capacity H_2 tank. By reducing the amount of yearly CO_2, it can be noted that the battery size decreases when hydrogen intervenes in the optimal HRES configuration (i.e., CO_2 lower than around 40 t/yr). When no CO_2 is released by the system, the battery capacity is 277 kWh in the BT+H_2 scenario, which is around 11 times lower than the size that is required in the BT scenario (i.e., 3,090 kWh). The hybrid storage case also needs smaller PV and WT sizes (Fig. 6b): in the DG-free case, the RES rated power is almost halved when switching from BT to BT+H_2 scenario. The hydrogen effectiveness relies also in the fact that, in H_2-based P2P systems, the storage capacity and power are decoupled and belonging to different components. Fig. 6c shows that the required FC and EL sizes are roughly constant, in the range of 80–90 kW and 105–115 kW, respectively. The H_2 tank capacity instead increases considerably up to about 718 kg when no diesel fuel is consumed (Fig. 6d).

Thus, the H_2-based P2P system is essential to achieve a cost-competitive solution, even though it has lower roundtrip efficiency (EL+FC) compared to batteries.

The ability of hydrogen to mitigate the LCOE rise is also clearly displayed in Fig. 7, where the LCOE breakdown is shown considering a diesel price of 2 €/L. By decreasing the diesel fuel consumption, the steep rise in LCOE of the BT scenario could be avoided with the inclusion of hydrogen: the cost contributions due to battery, photovoltaic and wind turbine systems (green, yellow and dark blue regions, respectively) remain almost constant, or even decrease, when hydrogen appears within the cost-optimal configuration (Fig. 7a). These contributions, instead, become increasingly relevant when trying to enhance the independence from fossil fuels by relying only on batteries as EES (Fig. 7b).

6. Conclusion

Cost-emission Pareto fronts have been developed for different configurations of stand-alone HRESs. The ε-constraint method was employed to address the multi-objective optimization problem. The proposed methodology was applied to a real off-grid insular community located in northern Europe.

When no constraints are imposed on the operation of the DG, the cheapest configuration consists of renewable generators (PV and WT), batteries and diesel genset. More specifically, DG is necessary to make the energy supply reliable and avoid the necessity of batteries with too large capacity. At the same time, batteries are required to better exploit the local RESs, thus reducing the system costs because of the lower fuel consumption.

By progressively enhancing the independence from fossil fuels, the inclusion of hydrogen in the HRES was shown to be essential to limit the increase in LCOE, even though its roundtrip efficiency is lower than that of batteries. This is because the cost-effective long-term storage capability of hydrogen allows the battery and the PV/WT systems not to be oversized. Considering the case with no diesel, the cost of energy of the BT+H_2 scenario is 0.41 €/kWh, which is approximately two thirds of the LCOE of the BT scenario. The battery capacity that is required in the hybrid storage case is roughly 11 times smaller than that of a system with only batteries. Moreover, the RES rated power is almost halved when switching from battery-only storage to hybrid battery-hydrogen storage. Renewable-based configurations were also found to be an economically feasible choice compared to an alternative solution based on sea cable replacement (whose cost is about 0.63 €/kWh).

To sum up, energy storage systems are key components to improve the independence from fossil fuels, with hydrogen playing an essential role in reducing the cost of energy.

Acronyms

AC	Alternating current
BOP	Balance of plant
BT	Battery
CT	Curtailed
DF	Diesel fraction
DG	Diesel generator
DST	Daylight saving time
DV	Decision variable
EA	Evolutionary algorithm
EES	Electrical energy storage
EL	Electrolyzer
EMS	Energy management strategy
EOT	Equation of time
FC	Fuel cell
GA	Genetic algorithm
HRES	Hybrid renewable energy system
HT	Hydrogen tank
LCOE	Levelized cost of energy
LD	Load
LOH	Level-of-hydrogen
LPSP	Loss of power supply probability
NOCT	Nominal operating cell temperature
NPC	Net present cost
OM	Operation and maintenance
PEM	Proton exchange membrane
PSO	Particle swarm optimization
PV	Photovoltaic
PVGIS	Photovoltaic geographical information system
P2P	Power-to-power
RES	Renewable energy sources
SOC	State-of-charge
STC	Standard test conditions
TMY	Typical meteorological year
UB	Upper boundary
UL	Unmet load
WT	Wind turbine

CRediT authorship contribution statement

Paolo Marocco: Conceptualization, Methodology, Software, Validation, Formal analysis, Investigation, Data curation, Writing – original draft, Visualization. **Domenico Ferrero:** Writing – review & editing, Supervision. **Andrea Lanzini:** Writing – review & editing, Supervision. **Massimo Santarelli:** Writing – review & editing, Supervision, Project administration, Funding acquisition.

Declaration of Competing Interest

The authors declare that they have no known competing financial interests or personal relationships that could have appeared to influence the work reported in this paper.

Acknowledgements

This project has received funding from the Fuel Cells and Hydrogen 2 Joint Undertaking under grant agreement No 779541. This Joint Undertaking receives support from the European Union's Horizon 2020 research and innovation program, Hydrogen Europe and Hydrogen Europe research.

Appendix A. Insight on PV power production

The total irradiance over the PV panel tilted surface was computed as follows [58]:

$$G(t) = G_{b,n}(t)\cdot cos(\theta) + G_{d,h}(t)\cdot F_{c,s} + G_{t,h}(t)\cdot \rho_g \cdot F_{c,g} \quad (A.1)$$

where $G_{b,n}$ (in kW/m^2) is the direct normal irradiance, $G_{d,h}$ (in kW/m^2) is the diffusive irradiance over the horizontal surface, $G_{t,h}$ (in kW/m^2) is the total irradiance over the horizontal surface, ρ_g is the ground albedo, $F_{c,s}$ is the collector-sky view factor, $F_{c,g}$ is the collector-ground view factor and finally θ is the angle of incidence to the tilted surface. The profiles of $G_{b,n}$, $G_{d,h}$ and $G_{t,h}$ were obtained from PVGIS tool [32], considering a typical meteorological year.

The terms $F_{c,s}$ and $F_{c,g}$ were determined in the following way:

$$F_{c,s} = \frac{1 + \cos(\beta)}{2} \quad (A.2)$$

$$F_{c,g} = \frac{1 - \cos(\beta)}{2} \quad (A.3)$$

where β represents the slope of the PV panel tilted surface, whose value (the optimal one) was taken from Ref. [32].

The angle of incidence (θ) was evaluated by applying the following relationship:

$$cos(\theta) = \cos(\beta)\cdot cos(\theta_z) + \sin(\beta)\cdot sin(\theta_z)\cdot cos(\phi_s - \phi) \quad (A.4)$$

where θ_z is the zenith angle, ϕ_s is the solar azimuth and ϕ is the PV panel surface azimuth (an optimal value, derived from PVGIS, was considered for ϕ).

The zenith angle (θ_z) parameter was defined as:

$$cos(\theta_z) = cos(\Phi)\cdot cos(\delta)\cdot cos(\omega) + sin(\Phi)\cdot sin(\delta) \quad (A.5)$$

where Φ is the latitude, δ is the declination and ω is the hour angle.

The declination can be derived by applying the approximated Cooper formula, which is function of the day of the year n as follows:

$$\delta = 23.45 \cdot sin\left(360 \cdot \frac{284 + n}{365}\right) \tag{A.6}$$

The hour angle was instead assessed as:

$$\omega = (h - h_{culm}) \cdot \frac{360}{24} \tag{A.7}$$

where h corresponds to the standard time, i.e., the time given by local clock and h_{culm} is the noon time, i.e., the time given by local clock when the sun is at its highest point above the horizon (crosses the local meridian).

The term h_{culm} is given by:

$$h_{culm} = 12 + \frac{L_{loc} - L_{ref}}{15} - \frac{EOT}{60} + DST \tag{A.8}$$

where L_{loc} is the longitude of the observer's meridian, L_{ref} is the longitude of the meridian for the local time zone, EOT (in minutes) is the equation of time and DST is the daylight saving time parameter (equal to 1 when in force and 0 otherwise).

Finally, the following expression was employed to assess the solar azimuth angle (ϕ_s):

$$cos(\phi_s) = \frac{cos(\theta_z) \cdot \sin(\Phi) - sin(\delta)}{sin(\theta_z) \cdot \cos(\Phi)} \tag{A.9}$$

Appendix B. Hydrogen storage

Fig. B.1 displays the LOH profile over the year for the 100% RES-based energy system. As reported in Table 3, the related HT size accounts for approximately 718 kg of hydrogen. It can be noted that the minimum value of LOH is around 0.11 (which corresponds to the LOH_{min} parameter set as input).;

To further investigate the role of H_2 in the HRES optimal design, the LCOE of the 100% RES-based energy system was evaluated as a function of the HT cost (see Fig. B.2). This cost was varied from 200 to 1100 €/kg to cover the range of 20 to 100 €/Nm^3 reported in Ref. [71]. Moreover, for the sake of completeness, the effect of the battery system cost (stack + BOP) was also analysed. As shown in Fig. B.2, hydrogen is confirmed to be fundamental to lower the LCOE across the entire range of HT and BT storage costs.

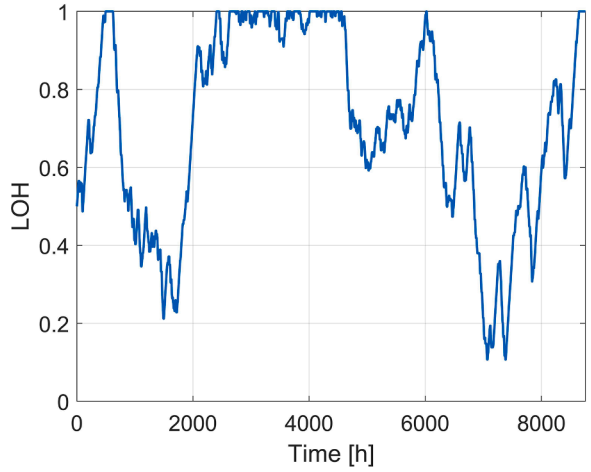

Fig. B.1. Level-of-hydrogen over the year for the 100% RES-based HRES.

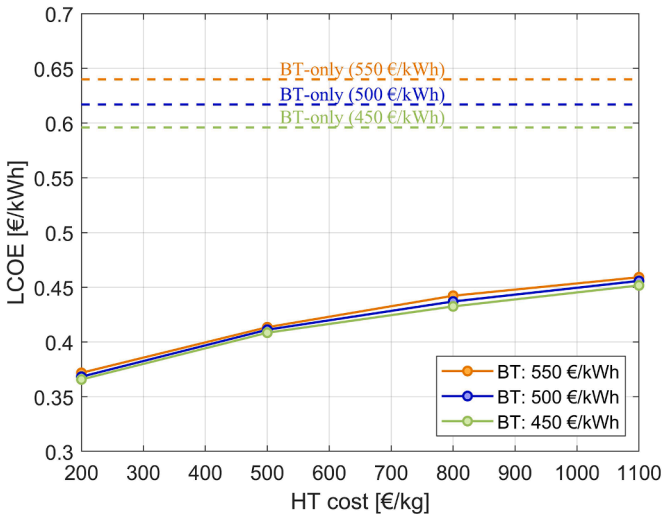

Fig. B.2. 100% RES-based HRES: LCOE as a function of the hydrogen tank cost for different values of cost of the battery. Solid lines refer to the LCOE of the HRES with hybrid storage, whereas dashed lines refer to a system configuration with only batteries as storage medium.

References

[1] P. Blechinger, C. Cader, P. Bertheau, H. Huyskens, R. Seguin, C. Breyer, Global analysis of the techno-economic potential of renewable energy hybrid systems on small islands, Energy Policy (2016) 1–14, https://doi.org/10.1016/j.enpol.2016.03.043.

[2] IRENA, Off-grid renewable energy solutions to expand electricity access: an opportunity, not to be missed (2019).

[3] IRENA, Off-grid renewable energy systems: status and, methodological issues (2015).

[4] P. Marocco, et al., A study of the techno-economic feasibility of H2-based energy storage systems in remote areas, Energy Convers. Manag. 211 (2020), 112768, https://doi.org/10.1016/j.enconman.2020.112768.

[5] S. Koohi-Fayegh, M.A. Rosen, A review of energy storage types, applications and recent developments, J. Energy Storage 27 (2020), 101047, https://doi.org/10.1016/j.est.2019.101047.

[6] S. Hajiaghasi, A. Salemnia, M. Hamzeh, Hybrid energy storage system for microgrids applications: a review, J. Energy Storage 21 (2019) 543–570, https://doi.org/10.1016/j.est.2018.12.017.

[7] Y. Yang, S. Bremner, C. Menictas, M. Kay, Battery energy storage system size determination in renewable energy systems: a review, Renew. Sustain. Energy Rev. 91 (January) (2018) 109–125, https://doi.org/10.1016/j.rser.2018.03.047.

[8] C. You, J. Kim, Optimal design and global sensitivity analysis of a 100% renewable energy sources based smart energy network for electrified and hydrogen cities, Energy Convers. Manag. 223 (April) (2020), 113252, https://doi.org/10.1016/j.enconman.2020.113252.

[9] A. Kovač, M. Paranos, D. Marciuš, Hydrogen in energy transition: a review, Int. J. Hydrogen Energy 46 (16) (2021) 10016–10035, https://doi.org/10.1016/j.ijhydene.2020.11.256.

[10] A. Malheiro, P.M. Castro, R.M. Lima, A. Estanqueiro, Integrated sizing and scheduling of wind/PV/diesel/battery isolated systems, Renew. Energy 83 (2015) 646–657, https://doi.org/10.1016/j.renene.2015.04.066.

[11] W. Cai, et al., Optimal sizing and location based on economic parameters for an off-grid application of a hybrid system with photovoltaic, battery and diesel technology, Energy 201 (2020), 117480, https://doi.org/10.1016/j.energy.2020.117480.

[12] H. Lund, P. Sorknæs, B.V. Mathiesen, K. Hansen, Beyond sensitivity analysis: a methodology to handle fuel and electricity prices when designing energy scenarios, Energy Res. Soc. Sci. 39 (2018) 108–116, https://doi.org/10.1016/j.erss.2017.11.013.

[13] O.D.T. Odou, R. Bhandari, R. Adamou, Hybrid off-grid renewable power system for sustainable rural electrification in Benin, Renew. Energy 145 (2020) 1266–1279, https://doi.org/10.1016/j.renene.2019.06.032.

[14] P. Marocco, D. Ferrero, A. Lanzini, M. Santarelli, Optimal design of stand-alone solutions based on RES + hydrogen storage feeding off-grid communities, Energy Convers. Manag. 238 (Jun. 2021), 114147, https://doi.org/10.1016/j.enconman.2021.114147.

[15] F. Dawood, G.M. Shafiullah, M. Anda, Stand-alone microgrid with 100% renewable energy: a case study with hybrid solar pv-battery-hydrogen, Sustain 12 (5) (2020), https://doi.org/10.3390/su12052047.

[16] P. Puranen, A. Kosonen, J. Ahola, Technical feasibility evaluation of a solar PV based off-grid domestic energy system with battery and hydrogen energy storage in northern climates, Sol. Energy 213 (2021) 246–259, https://doi.org/10.1016/j.solener.2020.10.089.

[17] O.V. Marchenko, S.V. Solomin, Modeling of hydrogen and electrical energy storages in wind/PV energy system on the Lake Baikal coast, Int. J. Hydrogen Energy 42 (15) (2017) 9361–9370, https://doi.org/10.1016/j.ijhydene.2017.02.076.

[18] H. Kalantari, S.A. Ghoreishi-Madiseh, A.P. Sasmito, Hybrid renewable hydrogen energy solution for application in remote mines, Energies 13 (23) (2020), https://doi.org/10.3390/en13236365.

[19] H.M. Ridha, C. Gomes, H. Hizam, M. Ahmadipour, A.A. Heidari, H. Chen, Multi-objective optimization and multi-criteria decision-making methods for optimal design of standalone photovoltaic system: a comprehensive review, Renew. Sustain. Energy Rev. 135 (April 2020) (2021), 110202, https://doi.org/10.1016/j.rser.2020.110202.

[20] M. Nunes Fonseca, E. de Oliveira Pamplona, A.R. de Queiroz, V.E. de Mello Valerio, G. Aquila, S. Ribeiro Silva, Multi-objective optimization applied for designing hybrid power generation systems in isolated networks, Sol. Energy 161 (2018) 207–219, https://doi.org/10.1016/j.solener.2017.12.046.

[21] A.L. Bukar, C.W. Tan, L.K. Yiew, R. Ayop, W.S. Tan, A rule-based energy management scheme for long-term optimal capacity planning of grid-independent microgrid optimized by multi-objective grasshopper optimization algorithm, Energy Convers. Manag. 221 (June) (2020), 113161, https://doi.org/10.1016/j.enconman.2020.113161.

[22] M.R. Quitoras, P.E. Campana, C. Crawford, Exploring electricity generation alternatives for Canadian Arctic communities using a multi-objective genetic algorithm approach, Energy Convers. Manag. 210 (2020), 112471, https://doi.org/10.1016/j.enconman.2020.112471.

[23] C.D. Rodríguez-Gallegos, D. Yang, O. Gandhi, M. Bieri, T. Reindl, S.K. Panda, A multi-objective and robust optimization approach for sizing and placement of PV and batteries in off-grid systems fully operated by diesel generators: an Indonesian case study, Energy 160 (2018) 410–429, https://doi.org/10.1016/j.energy.2018.06.185.

[24] M.J. Mayer, A. Szilágyi, G. Gróf, Environmental and economic multi-objective optimization of a household level hybrid renewable energy system by genetic algorithm, Appl. Energy 269 (2020), 115058, https://doi.org/10.1016/j.apenergy.2020.115058.

[25] F. Fodhil, A. Hamidat, O. Nadjemi, Potential, optimization and sensitivity analysis of photovoltaic-diesel-battery hybrid energy system for rural electrification in Algeria, Energy 169 (2019) 613–624, https://doi.org/10.1016/j.energy.2018.12.049.

[26] T. Tezer, R. Yaman, G. Yaman, Evaluation of approaches used for optimization of stand-alone hybrid renewable energy systems, Renew. Sustain. Energy Rev. 73 (December 2016) (2017) 840–853, https://doi.org/10.1016/j.rser.2017.01.118.

[27] M. Sharafi, T.Y. ELMekkawy, Multi-objective optimal design of hybrid renewable energy systems using PSO-simulation based approach, Renew. Energy 68 (2014) 67–79, https://doi.org/10.1016/j.renene.2014.01.011.

[28] T. Kerdphol, K. Fuji, Y. Mitani, M. Watanabe, Y. Qudaih, Optimization of a battery energy storage system using particle swarm optimization for stand-alone microgrids, Int. J. Electr. Power Energy Syst. 81 (2016) 32–39, https://doi.org/10.1016/j.ijepes.2016.02.006.

[29] REMOTE project official website (2018). https://www.remote-euproject.eu/. accessed May 30, 2021.

[30] A. Kafetzis, C. Ziogou, K.D. Panopoulos, S. Papadopoulou, P. Seferlis, S. Voutetakis, Energy management strategies based on hybrid automata for islanded microgrids with renewable sources, batteries and hydrogen, Renew. Sustain. Energy Rev. 134 (April) (2020), 110118, https://doi.org/10.1016/j.rser.2020.110118.

[31] J.J. Hwang, L.K. Lai, W. Wu, W.R. Chang, Dynamic modeling of a photovoltaic hydrogen fuel cell hybrid system, Int. J. Hydrogen Energy 34 (23) (2009) 9531–9542, https://doi.org/10.1016/j.ijhydene.2009.09.100.

[32] "Photovoltaic Geographical Information System (PVGIS)." https://ec.europa.eu/jrc/en/pvgis (accessed Mar. 11, 2021).
[33] M.K. Deshmukh, S.S. Deshmukh, Modeling of hybrid renewable energy systems, Renew. Sustain. Energy Rev. 12 (1) (2008) 235–249, https://doi.org/10.1016/j.rser.2006.07.011.
[34] M. Götz, et al., Renewable Power-to-Gas: a technological and economic review, Renew. Energy 85 (2016) 1371–1390, https://doi.org/10.1016/j.renene.2015.07.066.
[35] P. Trinke, P. Haug, J. Brauns, B. Bensmann, R. Hanke-Rauschenbach, T. Turek, Hydrogen Crossover in PEM and Alkaline Water Electrolysis: mechanisms, Direct Comparison and Mitigation Strategies, J. Electrochem. Soc. 165 (7) (2018) F502–F513, https://doi.org/10.1149/2.0541807jes.
[36] P. Marocco, et al., Online measurements of fluoride ions in proton exchange membrane water electrolysis through ion chromatography, J. Power Sources 483 (2021), 229179, https://doi.org/10.1016/j.jpowsour.2020.229179.
[37] H. Borhanazad, S. Mekhilef, V. Gounder Ganapathy, M. Modiri-Delshad, A. Mirtaheri, Optimization of micro-grid system using MOPSO, Renew. Energy 71 (2014) 295–306, https://doi.org/10.1016/j.renene.2014.05.006.
[38] R. Dufo-López, I.R. Cristóbal-Monreal, J.M. Yusta, Stochastic-heuristic methodology for the optimisation of components and control variables of PV-wind-diesel-battery stand-alone systems, Renew. Energy 99 (2016) 919–935, https://doi.org/10.1016/j.renene.2016.07.069.
[39] R. Dufo-López, L.A. Fernández-Jiménez, I.J. Ramírez-Rosado, J.S. Artal-Sevil, J. A. Domínguez-Navarro, J.L. Bernal-Agustín, Daily operation optimisation of hybrid stand-alone system by model predictive control considering ageing model, Energy Convers. Manag. 134 (2017) 167–177, https://doi.org/10.1016/j.enconman.2016.12.036.
[40] C.D. Barley, C.B. Winn, Optimal dispatch strategy in remote hybrid power systems, Sol. Energy 58 (4–6) (1996) 165–179, https://doi.org/10.1016/S0038-092X(96)00087-4.
[41] L. Gracia, P. Casero, C. Bourasseau, A. Chabert, Use of Hydrogen in Off-Grid Locations, a Techno-Economic Assessment, Energies 11 (11) (2018) 3141, https://doi.org/10.3390/en11113141.
[42] P. Rullo, L. Braccia, P. Luppi, D. Zumoffen, D. Feroldi, Integration of sizing and energy management based on economic predictive control for standalone hybrid renewable energy systems, Renew. Energy 140 (2019) 436–451, https://doi.org/10.1016/j.renene.2019.03.074.
[43] A. Brka, Y.M. Al-Abdeli, G. Kothapalli, Predictive power management strategies for stand-alone hydrogen systems: operational impact, Int. J. Hydrogen Energy 41 (16) (2016) 6685–6698, https://doi.org/10.1016/j.ijhydene.2016.03.085.
[44] A.Q. Jakhrani, A.R.H. Rigit, A.K. Othman, S.R. Samo, S.A. Kamboh, Estimation of carbon footprints from diesel generator emissions, in: *Proceedings of the 2012 International Conference in Green and Ubiquitous Technology, GUT 2012*, 2012, pp. 78–81, https://doi.org/10.1109/GUT.2012.6344193.
[45] P. Gabrielli, M. Gazzani, E. Martelli, M. Mazzotti, Optimal design of multi-energy systems with seasonal storage, Appl. Energy 219 (2018) 408–424, https://doi.org/10.1016/j.apenergy.2017.07.142.
[46] J. Kennedy, R. Eberhart, Particle swarm optimization, Proc. IEEE Int. Conf. Neural Netw. (1995) 1942–1948.
[47] J. Proost, State-of-the art CAPEX data for water electrolysers, and their impact on renewable hydrogen price settings, Int. J. Hydrogen Energy 44 (9) (2019) 4406–4413, https://doi.org/10.1016/j.ijhydene.2018.07.164.
[48] Battelle Memorial Institute, Manufacturing Cost Analysis of PEM Fuel Cell Systems for 5- and 10-kW Backup Power Applications (2016) [Online]Available, https://energy.gov/sites/prod/files/2016/12/f34/fcto_cost_analysis_pem_fc_5-10kw_backup_power_0.pdf.
[49] Tractebel and Hinicio, Study on early business cases for H2 in energy storage and more broadly power to H2 applications (2017) [Online]Available, https://www.fch.europa.eu/sites/default/files/P2H_Full_Study_FCHJU.pdf.
[50] U.S. Department of Energy, Hydrogen and Fuel Cell Technologies Office Multi-Year Research, Development, and Demonstration Plan - 3.3 Hydrogen Storage (2015). https://www.energy.gov/eere/fuelcells/downloads/hydrogen-and-fuel-cell-technologies-office-multi-year-research-development. accessed Sep. 11, 2021.
[51] Danish Energy Agency and Energinet, Technology Data - Energy storage (2018) [Online]Available, https://ens.dk/sites/ens.dk/files/Analyser/technology_data_catalogue_for_energy_storage.pdf.
[52] J. Gorre, F. Ruoss, H. Karjunen, J. Schaffert, T. Tynjälä, Cost benefits of optimizing hydrogen storage and methanation capacities for Power-to-Gas plants in dynamic operation, Appl. Energy 257 (May 2019) 2020, https://doi.org/10.1016/j.apenergy.2019.113967.
[53] M. Reuß, T. Grube, M. Robinius, P. Preuster, P. Wasserscheid, D. Stolten, Seasonal storage and alternative carriers: a flexible hydrogen supply chain model, Appl. Energy 200 (2017) 290–302, https://doi.org/10.1016/j.apenergy.2017.05.050.
[54] C. Bordin, H.O. Anuta, A. Crossland, I.L. Gutierrez, C.J. Dent, D. Vigo, A linear programming approach for battery degradation analysis and optimization in offgrid power systems with solar energy integration, Renew. Energy 101 (2017) 417–430, https://doi.org/10.1016/j.renene.2016.08.066.
[55] P. Marocco, D. Ferrero, E. Martelli, M. Santarelli, A. Lanzini, An MILP approach for the optimal design of renewable battery-hydrogen energy systems for off-grid insular communities, Energy Convers. Manag. 245 (2021), 114564, https://doi.org/10.1016/j.enconman.2021.114564.
[56] J.C. Alberizzi, J.M. Frigola, M. Rossi, M. Renzi, Optimal sizing of a Hybrid Renewable Energy System: importance of data selection with highly variable renewable energy sources, Energy Convers. Manag. 223 (2020), 113303, https://doi.org/10.1016/j.enconman.2020.113303.
[57] LG, LG NeON® R solar module (Mar. 11, 2021). https://www.lg.com/us/business/solar-panels/lg-LG365Q1C-A5. accessed.
[58] B. Laoun, A. Khellaf, M.W. Naceur, A.M. Kannan, Modeling of solar photovoltaic-polymer electrolyte membrane electrolyzer direct coupling for hydrogen generation, Int. J. Hydrogen Energy 41 (24) (2016) 10120–10135, https://doi.org/10.1016/j.ijhydene.2016.05.041.
[59] Wind Energy Solutions WES (2021). https://windenergysolutions.nl/.
[60] L. Moretti, M. Astolfi, C. Vergara, E. Macchi, J.I. Pérez-Arriaga, G. Manzolini, A design and dispatch optimization algorithm based on mixed integer linear programming for rural electrification, Appl. Energy 233–234 (2019) 1104–1121, https://doi.org/10.1016/j.apenergy.2018.09.194.
[61] Federal Ministry for Economic Affairs and Energy, Markets for Battery Storage. Sub-sector analysis on the market potential for battery storage in Tanzania (2015) [Online]Available, https://reiner-lemoine-institut.de/wp-content/publications/Battery_TZA/2015-en-battery-storage-tanzania.pdf.
[62] M.F. Zia, E. Elbouchikhi, M. Benbouzid, Optimal operational planning of scalable DC microgrid with demand response, islanding, and battery degradation cost considerations, Appl. Energy 237 (2019) 695–707, https://doi.org/10.1016/j.apenergy.2019.01.040.
[63] D. Ferrero, et al., REMOTE deliverable 1.4. First annual data reporting (2019).
[64] M. Santos, I. Marino, Energy analysis of the Raggovidda integrated system (2019) [Online]Available, https://www.haeolus.eu/wp-content/uploads/2019/01/D5.1.pdf.
[65] B. Li, R. Roche, A. Miraoui, Microgrid sizing with combined evolutionary algorithm and MILP unit commitment, Appl. Energy 188 (2017) 547–562, https://doi.org/10.1016/j.apenergy.2016.12.038.
[66] J.P. Torreglosa, P. García-Triviño, L.M. Fernández-Ramirez, F. Jurado, Control based on techno-economic optimization of renewable hybrid energy system for stand-alone applications, Expert Syst. Appl. 51 (2016) 59–75, https://doi.org/10.1016/j.eswa.2015.12.038.
[67] M. Boussetta, R. El Bachtiri, M. Khanfara, K. El Hammoumi, Assessing the potential of hybrid PV–Wind systems to cover public facilities loads under different Moroccan climate conditions, Sustain. Energy Technol. Assessments 22 (2017) (2017) 74–82, https://doi.org/10.1016/j.seta.2017.07.005.
[68] I. Tsiropoulos, D. Tarvydas, N. Lebedeva, Li-ion batteries for mobility and stationary storage applications (2018), https://doi.org/10.2760/87175.
[69] M.F. Shehzad, M.B. Abdelghany, D. Liuzza, V. Mariani, L. Glielmo, Mixed logic dynamic models for MPC control of wind farm hydrogen-based storage systems, Inventions 4 (4) (2019) 1–17, https://doi.org/10.3390/inventions4040057.
[70] TrønderEnergi, TrønderEnergi web site (Oct. 29, 2021). https://tronderenergi.no/. accessed.
[71] C. van Leeuwen, M. Mulder, Power-to-gas in electricity markets dominated by renewables, Appl. Energy 232 (July) (2018) 258–272, https://doi.org/10.1016/j.apenergy.2018.09.217.